Chemical Papers
https://doi.org/10.1007/s11696-022-02639-6

ORIGINAL PAPER

Synthesis, characterization, and application of external gelation of sodium alginate nanoparticles in molecular imprinting for separation and drug delivery of tenoxicam

Sumayha Muhammed Abbas[1] · Muhammed Emad Abood[2] · Rebwar Omar Hassan[3,4]

Received: 5 August 2022 / Accepted: 19 December 2022

Abstract
In this study, alginates, as the most versatile polymers, were employed to construct selective and effective molecular imprinted polymer (MIP) as a solid phase extraction adsorber for the estimation of tenoxicam (TNX) in pharmaceutical formulations. Based on the non-covalent approach, the polymerization reaction was performed with sodium alginate as a monomer, calcium chloride as a crosslinking reagent, and TNX as a template. The formed polymer was characterized by means of scanning electron microscopy (SEM), X-ray diffraction (XRD), differential scanning calorimetry (DSC), and Fourier transform infrared spectroscopy (FTIR). The distribution ratio results showed that the particle formed ranges were less than 100 nm. To evaluate binding capacity, batch binding assays were utilized, and the results were monitored using UV–Vis spectroscopy at 369 nm. The drug delivery of the imprinted surface was studied in different acidic media that mimic the gastric medium, intestine and blood plasma. The results show that the best way to deliver drugs is in the acidic environment of the stomach.

Keywords Alginate · Tenoxicam (TNX) · Molecular imprinting · Drug delivery · Pharmaceutical products

Introduction

Molecularly imprinted polymers (MIPs) first appeared in research in the early 1990s of the previous century and have since grown in popularity. These synthetic polymeric materials, with specific receptor sites in their matrix, are one of the most promising separation techniques. MIPs are used in a wide range of applications as a separation technique for complicated matrices, as evidenced by the growing number of publications (Szatkowska et al. 2013; Hussein and Al-Bayati 2021; Al-Bayati and Al-Safi 2018; Al-Abbasi et al. 2020). These polymers are custom-made synthetic materials with artificially made recognition sites that can effectively bind a target compound even when other closely related compounds are present (Tamayo et al. 2007).

A molecular imprinting guest–host framework enables the embedding of specialized substrate recognition into a chemically synthesized polymeric matrix. Imprinting involves copolymerizing active monomers with a crosslinking agent in the presence of a template molecule. To generate a hard polymeric matrix, the polymerization process allows for a strong and sophisticated combination of both functional monomers and templates. After rinsing and elution, the resultant polymer matrix is left with cavities that are similar in spatial organization and molecular interaction to template molecules, resulting in high affinity, selectivity, and recognition toward the target template (Sarpong et al. 2019, Abood and Abbas, 2021).

Currently, the emphasis is on employing low-cost, environmentally friendly materials. Furthermore, natural components are becoming extremely prevalent in food, pharmaceuticals, and cosmetics, according to recent trends. The hydrocolloid alginate is a biodegradable and biocompatible co-polymer of guluronic acid and mannuronic acid that has already received FDA approval for human use (Ahmad

✉ Rebwar Omar Hassan
rebwar.hassan@su.edu.krd

[1] Department of Chemistry, College of Education for Pure Science Ibn Al-Haitham, University of Baghdad, Baghdad, Iraq

[2] Ministry of Education, Baghdad Educational Rusafa Directorate I, Baghdad, Iraq

[3] Department of Chemistry, College of Science, Salahaddin University, Erbil-kurdistan region, Iraq

[4] Medical Analysis Department, Applied Science Faculty, Tishk International University, Erbil-kurdistan region, Iraq

Published online: 27 December 2022

et al. 2006; Alkhatib et al. 2020). Because of its low toxicity, low cost, and moderate gelation by the addition of divalent cations (Ca^{2+}), a naturally occurring anionic polymer (biomaterial), alginate, has been extensively explored and employed for numerous biomedical science and engineering applications (Cetinkaya et al. 2022; Gao et al. 2022; Hamed et al. 2017). It has a number of attractive biopharmaceutical features, including pH sensitivity, biodegradability, mucoadhesiveness, and non-immunogenicity, making it a good candidate for modified drug release (Prabaharan 2015; Hasseb et al. 2022). As a consequence, the researchers considered employing materials with these properties in the synthesis of molecular imprinting polymers to separate vital materials such as proteins (Herrero et al. 2010; Qi et al. 2019; Liu et al. 2018), and different chemical compounds (Zhao et al. 2014; Chen et al. 2010).

The past century's achievements, mainly the discovery of life-saving drugs, led to a dramatic improvement in healthcare. The use of drug delivery systems (DDS) is one method for improving the therapeutic effects of medications. As attractive and efficient materials, molecular imprinted polymers (MIPs) are a promising candidate for drug delivery. MIPs are one of the greatest materials for use as a scavenger in DDS because of their capacity to release a reliable result of drug carrier that is proportional to increased loading susceptibility and intelligent release of the therapeutic (Mokhtari and Ghaedi 2019). One of the major qualities necessary for the optimal design of therapeutic agents for oral administration is the release of an imprinted molecule in response to changes in the acidity of the surrounding medium (Ciurba et al. 2021b). Additionally, its excellent alternatives in the area of DDS are alginate MIP as pH-sensitive polymer hydrogels with such a polymeric network that is able to take or donate protons at a given pH, through a volume phase transition from a collapsed state to an extended one (Puoci et al. 2008; Kurczewska 2022).

Tenoxicam (TX) (4-hydroxy-2-methylthieno[2,3-e][1,2]thiazine-3-carboxylic acid 1,1-dioxide) (Fig. 1) is a non-steroidal anti-inflammatory drug (NSAID) (Ciurba et al. 2021a). It is rather frequently prescribed because it specifically inhibits COX-2 (cyclo-oxygenase enzyme), which could mean that negative side effects such as gastric acidity occur less often (Arslan et al. 2011). Given the importance of this drug, a review of the literature reveals various methods for estimating TNX, including spectrophotometers (Amin 2002), HPLC (Madni et al. 2016), flow injection analysis (Chen and Zhao 2012), and the voltammetry method (Demiralay and Yılmaz, 2012).

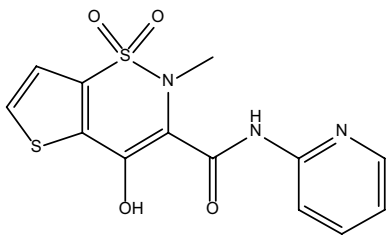

Fig. 1 Chemical structure of tenoxicam

The objective of this study was to develop a non-covalent interaction procedure for the manufacture of nanoscale molecular imprinting polymer (MIP) consisting of alginate as the monomer, divalent metal (Ca^{2+}) as the crosslinker, and TNX as the template. The synthesized MIP was then employed in the solid phase extraction of the tenoxicam drug in bulk and pharmaceutical products, which was afterward evaluated spectrophotometrically. In a second part of this study, the capabilities of fabricated MIP nanoparticles as drug delivery vehicles were evaluated using in vitro release tests in varying pH ranges that mimic body fluids (Fig. 2).

Experimental

Materials

Tenoxicam powder in a pure form (99.99%) was obtained from Middle East Pharmaceutical Manufacturing Co. Ltd., Iraq. All of the chemicals used were of analytical grade, and they were utilized just as they were received, with no further purification.

Procaine (PRO) was bought from the state company for drugs industry and medical appliances (SDI), Iraq. Niclosamide, K_2HPO_4, and Na_2HPO_4 were purchased from Sigma-Aldrich Co. Ltd. (USA). To simulate stomach juices, a buffer solution (pH 1) was made by adding 0.83 mL of HCl to a 50-mL volumetric flask and then filling the flask to the mark with distilled water.

Preparation of MIP and NIP

In order to prepare the nanoaggregate particles for molecular imprinting (MIP), 1.0 g of sodium alginate and 0.04 g of TNX template are dissolved in 20 mL of distilled water and stirred to ensure the dissolution of alginate and TNX template. This takes 120-min period. Separately, 3.0 g of $CaCl_2$ was dissolved in 20 mL of distilled water in a second flask. The dissolved $CaCl_2$ salt was added to the alginate-TNX mixture and stirred for a further 60 min. Then, 40 mL of methanol was added to accelerate the synthesis of hydrocolloid alginate particles of MIP. After polymerization, the excess amount of solvent was removed by centrifugation of the resulting suspension solution.

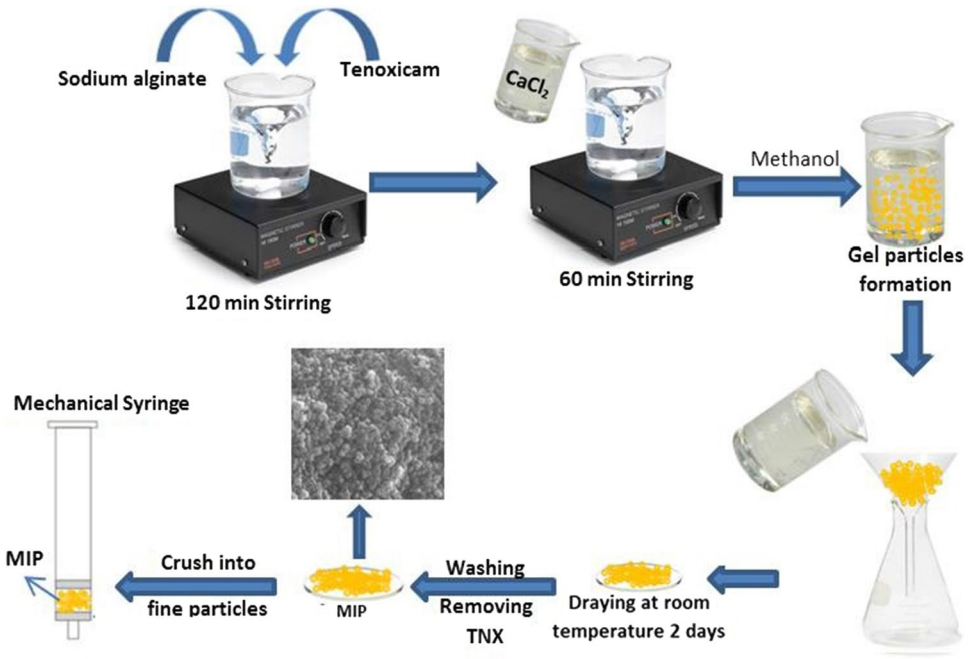

Fig. 2 Schematic illustration of alginate-based MIP synthesis and application

Elution of TNX template

The printed template (TNX) was removed from the MIP polymer by repeatedly washing them in an ultrasonic bath (SONOREX-Germany) for 30 min with a 15 mL solution of methanol and acetic acid (3:1), leaving merely a molecular imprint polymer (MIP). Each time, after centrifugation, the absorbance of the supernatant solution was monitored by UV–Vis spectrophotometer (UV-1900i Shimadzu) at 369 nm to verify that the release process was completed and that the resulting MIP polymer was empty of the TNX templates. The synthesized MIP particles were then collected, filtered, and air-dried for two days at room temperature. The obtained nanopolymer (MIP) was ground and used for sorption and desorption process in subsequent studies. As a reference, non-imprinted polymer (NIP) was prepared using an identical procedure but without the template (TNX).

Pharmaceutical sample preparation

The sample preparation procedure includes mixing the contents of 10 capsules, weighing a portion of the sample in which the amount of TNX is equivalent to 0.01 g mixed with distilled water using an ultrasonic bath, until the powder is completely disintegrated and the resultant solution is allowed to settle. The solution was filtered, and the insoluble residue was washed several times with distilled water. Then the washing was added to the filtrate and diluted to a volume of 100 mL in a volumetric flask to obtain a 100 µg mL-1 stock solution. Then, from the stock solution, three different volumes (0.7, 1.0, and 1.3 mL) were taken and placed in a 10-mL volumetric flask and diluted with distilled water.

Drug delivery study

Drug loading

0.5 g of polymeric matrix was immersed in 10 mL of TNX solution (10 µg/L) and stirred continuously for 4 h at room temperature. After that, the solvent was removed, and the powder was left at room temperature for two days to dry.

Buffer media

A buffer solution with pH 6.8 was prepared by mixing 10.2 mL of sodium phosphate monobasic (monohydrate) (0.5 mol/L) with 9.8 mL of sodium phosphate dibasic (heptahydrate) (0.5 mol/L) solution and adjust the final volume to 200 mL with distilled water (simulate intestinal fluids). Buffer solution (pH 7.4)-simulated blood plasma was prepared by mixing 3.8 mL of sodium phosphate monobasic (monohydrate) (0.5 mol/L) with 16.2 mL of sodium phosphate dibasic (heptahydrate) (0.5 mol/L) solution and adjust the final volume to 200 mL with distilled water (Chandra Mohan 2003). To simulate stomach juices, a solution of pH 1.0 was made by adding 0.83 mL of HCl to a 5-mL volumetric flask and then filling the flask to the mark with distilled water.

Release of drugs in vitro

Tenoxicam (TNX) in vitro delivery behavior from MIP was investigated in different pH media to determine how these media could alter the TNX behavior under different conditions. The experiment was carried out in a 50-mL solution containing 10 µg.L^{-1} of TNX at three release pH values (1.0, 6.8, and 7.4) with continuous stirring at 37 °C. To keep the pH constant, 3.5 mL of the sample was taken at specified time intervals and replaced with an equal volume of pH buffer. The amount of TNX emitted at specific periods was measured spectrophotometrically at 369 nm. The Higuchi model, in accordance with Eq. 5, was used to investigate the TNX release mechanism from MIP by plotting the cumulative percentage of drug (%CRR) released against the square root of time.

Adsorption equations

In five batches, 0.5 g of MIP and NIP was weighed and placed in a separation column, in which they were activated with 10 mL of distilled water. Then a 10 mL solution of 10 µg mL^{-1} TNX was added into the column, followed by a 10-min equilibrium time. The solution extracted from the column was collected in a 10-mL volumetric flask after the column was mechanically squeezed. A UV–Vis spectrophotometer set at 369 nm was used to measure the absorption at room temperature**.** The binding capacity of TNX and MIP was calculated based on the following equation:

$$Q = \frac{(C_o - C_e)V}{W} \tag{1}$$

Q (µg.g^{-1}) is referred to the binding capacity for the MIP, C_o (µg mL^{-1}) is the concentration of template in the solution before contact with the polymer, V is the template solution's volume (mL), C_e (µg mL^{-1}) is the equilibrium concentration of the template in the solution phase, W (g) referred to the polymer dry mass MIP (g).

The interaction between the template and adsorbent active sites is estimated using the Scatchard equation (as a linearized formulation of the Langmuir adsorption isotherm) according to the following equation (Jaoued-Grayaa et al. 2022; Scatchard 1949):

$$\frac{Q}{C_e} = \frac{Q_{max} - Q}{K_d} \tag{2}$$

in which Q_{max} refers to the maximum binding capacity of the template (TNX), C_e (µg mL^{-1}) is the remained analytical concentration of the TNX template at equilibrium, and K_d is the dissociation constant; division constant correlated with adsorption site attraction.

The specific adsorption is the ratio of MIP Q_{max}(µg.g^{-1}) adsorption capacity to that of its NIP counterpart Q_{max} (µg.g^{-1}). The imprinting factor (IF) determined according to Eq. 3 which defines this feature (Nantasenamat et al. 2007; Decompte et al. 2020).

$$IF = \frac{Q_{max}(MIP)}{Q_{max}(NIP)} \tag{3}$$

Finally, the cumulative release rate (% CRR) was determined using the following equation (Zhang et al. 2017a):

$$\%CRR = \left(\frac{M_t}{M_\infty}\right)x100 \tag{4}$$

where M_t the total amount of TNX is released at time t, and M_∞ is the total quantity of TNX impregnated in the MIP at an endless time.

The in vitro release performance of TNX from MIPs was assessed using the release kinetics equations of the frequently used mathematical *Higuchi* model (Eq. 5).

$$\left(\frac{M_t}{M_\infty}\right) = K_H\sqrt{t} \tag{5}$$

where $\left(\frac{M_t}{M_\infty}\right)$ is the release percentage (%),K_H is the *Higuchi* release rate constant, and t is the release time (Zhu et al. 2017).

Statistical analysis

All studies were performed in triplicate, and results were reported as means ± SD. A one-way analysis of variance was used to determine the significance of data variances in all obtained results, at a significance level of smaller than 5%.

Results and discussion

Characterization

Scanning electron microscopy (SEM) (TESCAN MIRA III-Czech)

The morphological investigations (shape and size) of the NIP and MIP were carried out using SEM analysis. An SEM image has been taken at different magnifications. Figure 3 demonstrates that the polymer has a spherical shape and size in the nano-range, less than 100 nm. As a result, it can be applied as a nano-size adsorbent for more efficient extraction of TXN. The interaction between monomers and template in MIP results in a considerable difference in surface shape, and NIP has more regular partials in size, shape, and smaller size. When tenoxicam

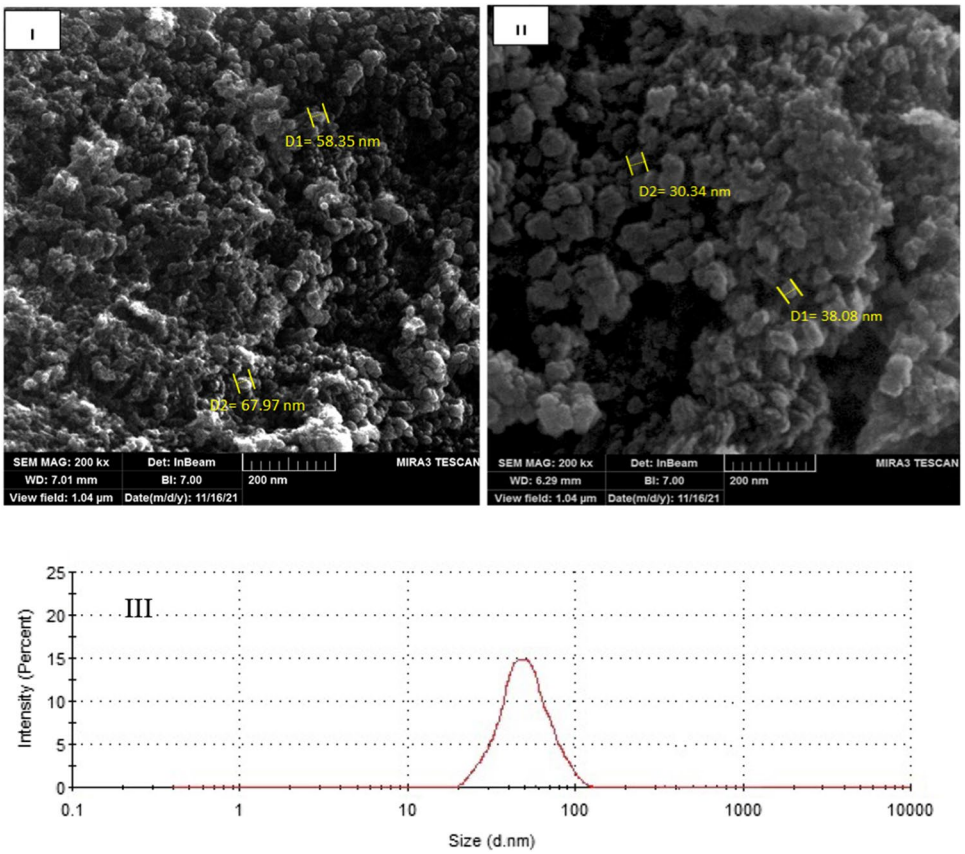

Fig. 3 SEM images of MIP (I) and NIP (II) and dynamic light scattering (DLS) graph(III)

(TNX) was added to the reaction mixture of alginate and calcium chloride, irregular and large nanoparticle sizes were observed. This can be explained by the fact that tenoxicam is an active oxygen scavenger in the monomer and has a low solubility in the aqueous reaction medium (El-Gazayerly 2000).

Dynamic light scattering (DLS) (particle size analyzer, SZ-100-HORIBA, Japan) was employed to measure the particle size and size distribution. Figure 3-III demonstrates that the particle size of MINPs is less than 100 nm.

X-ray diffraction (XRD-Shimadzu 6000)

The X-ray diffraction structures of NIP and MIP with TNX as a template are shown in Fig. 4. Two of the sharpest crystalline peaks 2θ are found at 20 and 40 in the X-ray pattern. When comparing MIP to NIP, the strength of each of these peaks was reduced, indicating the decreasing MIP crystallinity. This is due to the TNX template weakening the polymer's crystal structure and decreasing coherent layer scattering (Abdeen and Salahuddin 2013). Because of the interaction, the carboxyl group became a source of particle accumulation, and the pattern for MIP with the template became less intense.

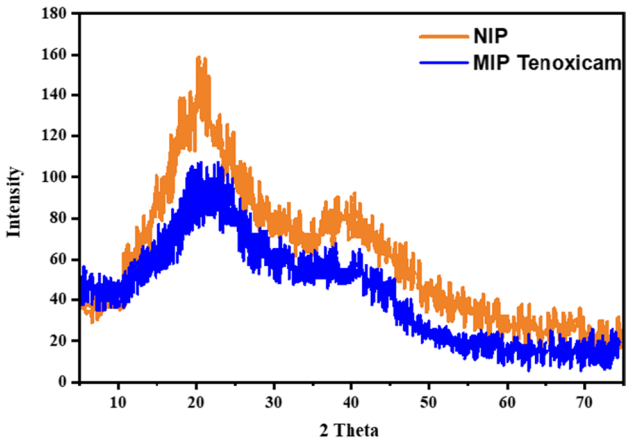

Fig. 4 Illustrate X-ray diffraction pattern by Cu K_α radiation ($\lambda = 1.54060$ Å) of NIP and MIP -TNX

Fourier transform infrared spectroscopy (FTIR-IRTracer-100- Shimadzu)

According to stretching vibrations of the polysaccharide's characteristic hydroxyl group, both the NIP and MIP spectra exhibit a significant broad band around 3421 cm^{-1}, which can be attributed to intermolecular hydrogen

bonding between various alginate molecules (Fig. 5). In the presence of TNX, the monomeric carboxylic acid group's C = O stretching mode shifts from 1647 cm^{-1} in NIP to 1635 cm^{-1} in MIP. The C = O stretching frequency of alginate is further lowered in the presence of TNX due to resonance stabilization (Geetha et al. 2016). A new band corresponding to the carboxyl group occurred at 1716 cm^{-1}, with MIP referring to the free group generated after mixing with TNX. It is self-evident that the bands relating to carboxylate groups can be utilized to correlate variations in the structure of different alginate polymers.

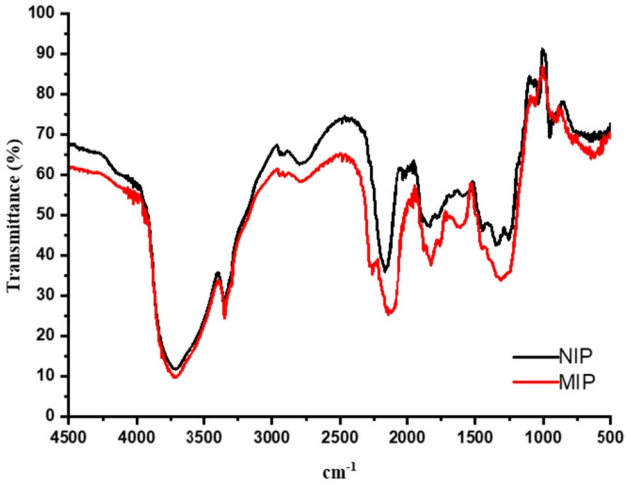

Fig. 5 FTIR spectrum of MIP and NIP

Differential Scanning Calorimetry (DSC-TA Instruments SDT-Q600)

Figure 6 displays a strong endotherm for NIP and MIP in the DSC thermogram study of calcium alginate, which reflects alginate decarboxylation and decomposition. While the alginate decomposition peak shifted to higher temperatures in MIP, the exothermic peak appeared at 296 °C, dependent on the hardening time of beads and the amount of crystalline TXN (Smrdel et al. 2006). The melting point of tenoxicam was also not apparent in the beads. It was most likely owing to the alginate exothermic decomposition and the tenoxicam decomposition endotherm overlapping (You et al. 2018).

Maximum wavelength and calibration curve

TNX concentrations ranging from 0.5 to 14.0 µg mL^{-1} were prepared by transferring various volumes of TNX from a standard solution of 100 µg mL^{-1} to a 10-mL volumetric flask and then filling the volume with distilled water. Absorption spectra and calibration curves are depicted in Figs. 7 and 8, respectively.

Experimental optimization

TNX template weight, alginate amount, $CaCl_2$ weight, and contact time, all of which affect the MIP's adsorption performance, were optimized by altering one parameter at a time while maintaining the other entire constant.

Three MIP polymers were synthesized using varied weights of TNX template to produce the polymer with the highest TNX content. The synthesized MIP, after leeching the template by the washing solvent, loaded with 10 µg mL^{-1}

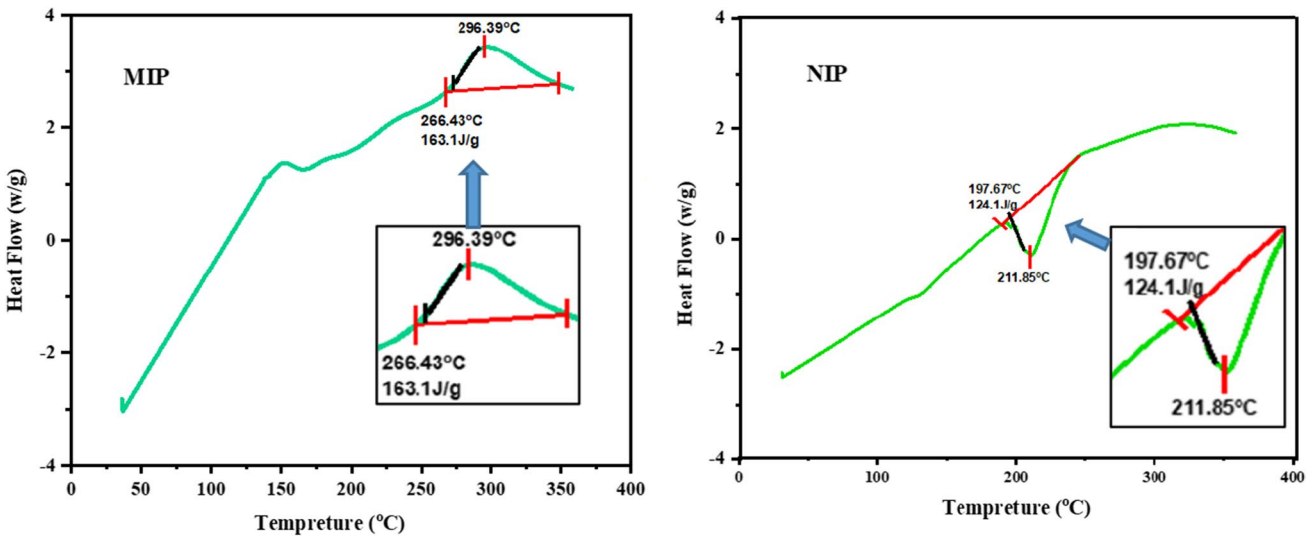

Fig. 6 DSC/TGA thermogram for NIP and MIP

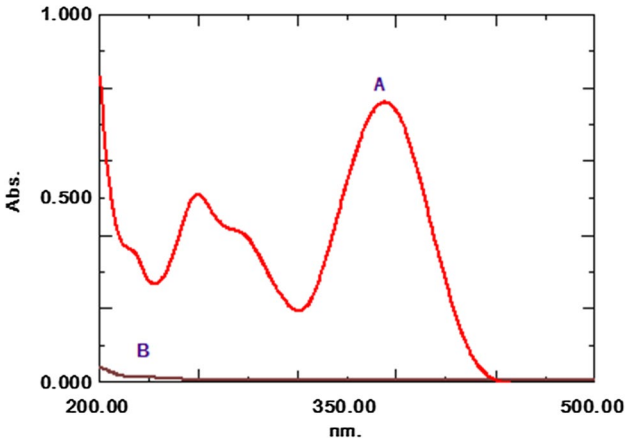

Fig. 7 Absorption spectrum of 10 μgmL^{-1} of TNX at 369 nm **A** against the blank solution **B**

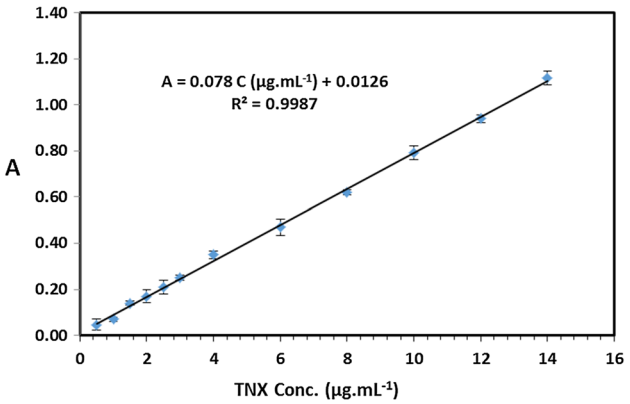

Fig. 8 Calibration curve linearity for TNX

TNX; after equilibration, an adsorbed TNX was monitored spectrophotometrically at 369 nm. It is clear that using a small amount of the template during MIP synthesizing results in a small number of TNX imprinting, and thus the amount of drug (TNX) remaining in the solution that is not adsorbed by the MIP is large when compared to what is available when using larger amounts of the template. Otherwise, when higher amount of templates were used, a negative effect was detected. Table 1 shows that 0.04 g yields the maximum binding capacity (Q) of 171 μg g^{-1}, which was preserved and utilized in the following experiments.

Three MIP polymers were synthesized with varying weights of sodium alginate (ALG). After rinsing the template, it was then applied to extract TNX solution containing 10 μg mL^{-1}. The results show that as the concentration of ALG increased, the binding capacity (Q) of TNX–MIP improved, and the highest value of Q (171.67 μg g^{-1}) was found with 1.0 g of ALG (Table 2). It was attributed to the fact that as the concentration of ALG increased, more hybrid complex components were generated, resulting in an increase in the number of imprinting holes (Ciurba et al. 2021a). The reduction in sodium alginate polymer chains and hydroxyl groups that are attached to the calcium cation was related to a decrease in alginate concentration, which resulted in a reduction in MIP mean particle size. More functional groups can congregate around calcium crosslinking agents as alginate concentration increases, allowing for more layers of alginate chains to connect the calcium cations. Finally, as the concentration of alginate increases, the size of MIP nanoparticles grows (Daemi and Barikani 2012).

Sodium alginate is a linear homo-polymer that may crosslink with various multivalent cations, such as Zn^{2+}, Fe^{3+}, and Ca^{2+} (Wu et al. 2019; Chan et al. 2002). The Ca ions, on the other hand, are preferred because it selectively binds the alginate liner polymer at various places, resulting in egg-box forms (Shalapy et al. 2020; Rastogi et al. 2007). As a result, the amount of Ca^{2+} utilized as a crosslinker influences the spherical form, size, entrapment ability, and harder texture of the alginate polymer (Haldar and Chakraborty 2019). Accordingly, to probe the effects of Ca ion, three separate MIP samples were made, each with a different amount of $CaCl_2$. The extraction of a 10 g.mL^{-1} TNX solution was carried out. The results reported in Table 3 revealed that 3.00 g of $CaCl_2$ has the best binding capacity of 175.40 μg.g^{-1}. The higher the $CaCl_2$ concentration, the more TNX leaks along with water during the polymer's progress, making it difficult to elute and increasing the binding capacity (Arslan et al. 2011).

Effect of MIP weight

The MIP was weighed at various weights ranging from 0.1 to 0.7 g, and the extraction process was performed under optimal conditions. According to the results in Table 4, the greatest binding capacity of 175.4 μg.g^{-1} was obtained with 0.50 g of MIP. Q values remain constant at higher weights. This is owing to the saturation of the selective cavities in MIP (Bereli et al. 2020).

Effect of temperature

At different temperature, various MIP and NIP models were developed, and under identical conditions, MIP and NIP separation methods were carried out. The temperature of 50 °C was found to have the best binding capacity of 192.0 μg.g^{-1}. Modification in TNX cavity size, hydrophobic interaction, and hydrogen bonding interaction were all linked to changes in binding capacity (Q) with temperature. With temperature rising from 10 to 50 °C, there is a clear inclination that the cavity size of the polymers increased, resulting in an increase in Q values, which enables the approximation of TNX molecules to the specific holes (Fig. 9).

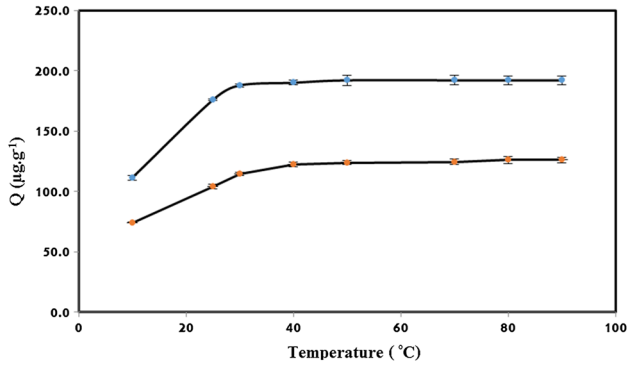

Fig. 9 Isotherm curves for the adsorption of TNX on MIP **a** and NIP **b**

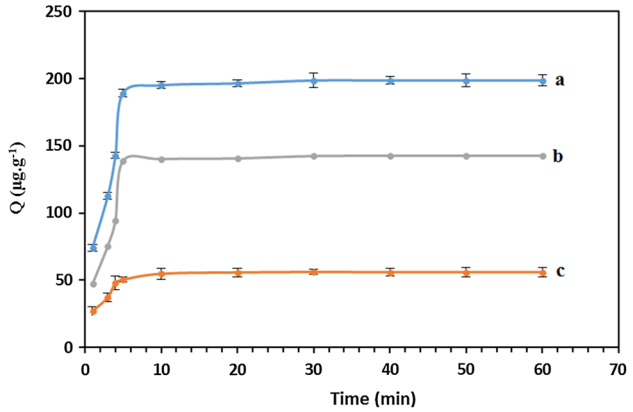

Fig. 10 Dynamic adsorption curves of the MIP **a** and NIP **b** to TNX and Δ*Q* (MIP-NIP) **c**

Effect of equilibrium time

The extraction process was performed with different equilibrium times for the same TNX concentration (10.0 μg mL^{-1}) under the same conditions. The best binding capacity (198.56 $g.g^{-1}$) was achieved using a 30-min equilibration time, which was used in further studies.

The dynamic adsorption curves of the MIP and NIP were recognized by observing the concentration of TXN during a time period of 1 to 60 min. The Q values of the MIP increased rapidly in the first 5 min, and the equilibrium was established at about 10 min, as shown in Fig. 10, while remaining almost unaffected from 10 to 60 min, indicating that the adsorption of TNX on the MIP was saturated and stabilized. The specific adsorption (ΔQ) of TNX by MIP increased with time, revealing that the imprinting procedure was effective. These results show that MIP can be used to move TNX so that it can be adsorbed and separated.

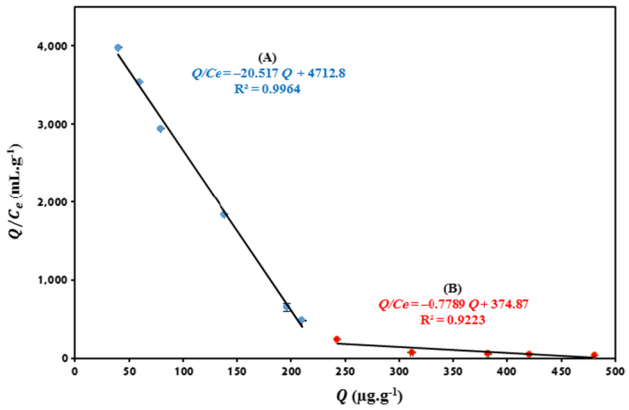

Fig. 11 Scatchard plot showing TNX adsorption on MIP, with high affinity sites **A** and low affinity sites **B**

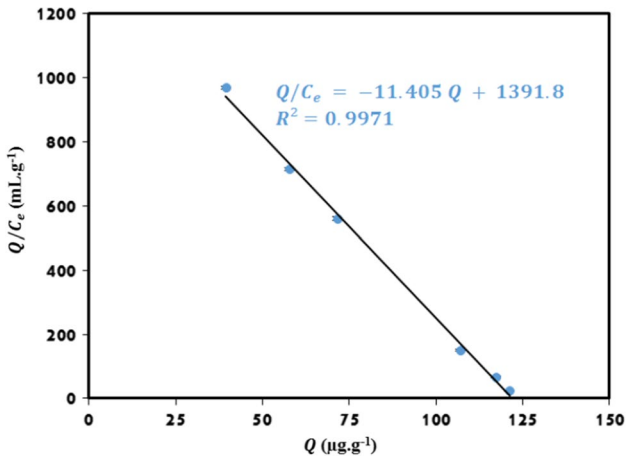

Fig. 12 Scatchard plot showing TNX adsorption on NIP

Scatchard plot study

Scatchard plots, which are useful for measuring adsorption sites, were used to further analyze the binding capacity. The Scatchard plot for MIP in Fig. 11 showed two discontinuous lines with different distinct slopes: one for the high affinity site with the regression equation $\frac{Q}{C_e} = -20.517Q + 4712.8\left(R^2 = 0.9964\right)$ and one for the low affinity site $(\frac{Q}{C_e} = -0.7789Q + 3374.87)$ $\left(R^2 = 0.9223\right)$. This demonstrated that there were two types of binding sites in the MIP able to adsorb TNX (surface sites and cavities). In contrast to MIP, for NIP the plot of Q/C_e against C_e in Fig. 12 showed only one line with regression equation $\frac{Q}{C_e} = -11.405Q + 1391.8$ $(R^2 = (0.9971)$. Table 5 shows the estimated K_d and Q_{max} values for MIP and NIP based on the negative slope and intercept of the regression equations (Zhang et al. 2017b; Hou et al. 2014). NIPs had a lower capacity for adsorption than MIPs. This could be due to the

fact that in the absence of template molecules, the NIP was unable to create voids and binding sites for the selective adsorption of TNX. The NIPs, on the other hand, can adsorb TNX molecules through non-selective surface sites via intermolecular interactions like Van der Waals forces. Scatchard plots only revealed the existence of two types of MIP binding sites and only one type of NIP binding site, according to a basic interpretation (Jaoued-Grayaa et al. 2022).

The main strength of the polymer binding with the template is due to the formation of non-covalent interactions like hydrogen bonds between the template atoms represented in nitrogen, oxygen, and sulfur with what is on the polymer (chemical adsorption). This is in addition to the existing and printed cavities in the shape of the TNX in MIP that are not present in the case of the NIP. Slightly, both polymers are equal in their active centers located on the surface (physical adsorption). Thus, it can be said that the binding opportunities in the case of the MIP of target molecules are greater than those present in the case of the NIP (Zhang et al. 2018; Huang et al. 2018).

Selectivity

This study was carried out to determine the extent to which the MIP is selective toward the TNX when compared to the NIP, in which, in a 10-mL volume flask, 10 µg mL^{-1} TNX was mixed with 10 µg mL^{-1} procaine (PRO) and niclosamide (NIC) independently to make two distinct solutions. The tenoxicam presence in the two different matrixes was separated, and then the recovery of the drug retained in the MIP and NIP was computed. Table 6 shows that MIP has a preferential propensity to tenoxicam, with a recovery rate of 84.54% compared to 38% in NIP.

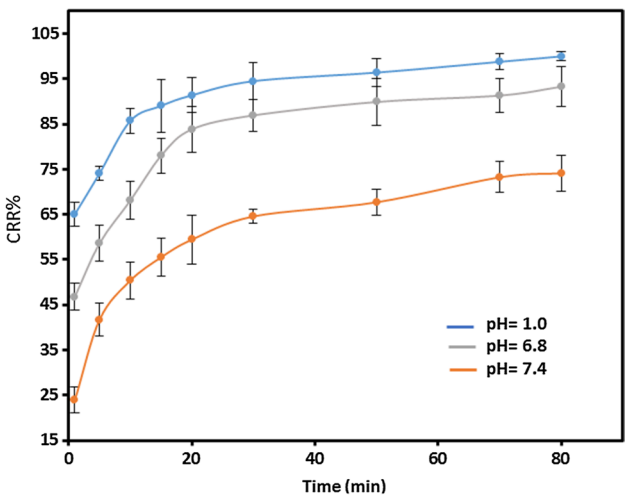

Fig. 13 TNX-MIP release curve at various pH mediums

In vitro drug release study

To demonstrate the effect of pH on the release process from the polymer, the cumulative release rate (Eq. 4) of TNX drug from MIP was measured at various pH values. Three solutions were prepared: one with a pH of 1 to resemble stomach fluids, another with a pH of 6.8 to simulate intestinal fluids, and a third with a pH of 7.4 to simulate blood plasma. MIP was used to extract a 10 µg mL^{-1} TNX solution, after which the MIP was placed in buffer solutions with different pH (1, 6.8, and 7.4) and the TNX concentrations were measured in the solution over time at 37 °C ± 1. The results in Fig. 13 reveal that the release rate was identical for all of the pH values examined, starting with a 20-min initial release followed by an 80-min steady release.

The release kinetics curve of MIPs for TMX at pH = 6.8 and 7.4 fits to the *Higuchi* mathematical model, as illustrated in Fig. 14 and Table 7, demonstrating that the release of MIPs for TNX follows Fick's law. The linear (R^2) regression coefficient value of the fitted line can be used to estimate the drug release mechanism. First, because MIPs have a limited number of TNX imprinting sites on their surfaces, MIPs loaded with TNX released TNX to the buffer at a steady rate over a fixed length of time (rather than in a burst release). The TNX

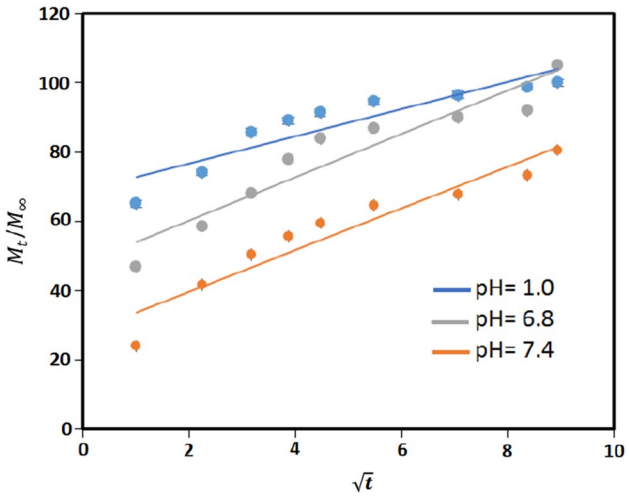

Fig. 14 TNX release in vitro according to the *Higuchi* model at various pH levels

Table 1 The influence of TNX mass on MIP binding capacity

TNX (g)	C_e(µg mL^{-1}) ±*SE*;*SD**	RSD	Q(µg g^{-1})
0.03	2.66 ± 0.028; 0.049	1.857	146.87
0.04	1.45 ± 0.015; 0.025	1.740	171.07
0.05	3.71 ± 0.018; 0.031	0.824	125.87

*SE refers to the standard error, and SD was the standard deviation for three replicate experiments ($n = 3$).

Table 2 The effect of alginate weight

Alginate (g)	C_e(μg mL^{-1}) ± SE, SD (n = 3)	RSD	Q(μg g^{-1})
0.5	3.09 ± 0.030; 0.052	1.682	138.20
1.0	1.42 ± 0.009; 0.015	1.078	171.67
2.0	1.45 ± 0.007; 0.012	0.795	170.93

Table 3 Study the effect of $CaCl_2$ weight on the binding capacity

$CaCl_2$ (g)	C_e(μg mL^{-1}) ± SE; SD (n = 3)	RSD	Q(μg g^{-1})
1.0	1.45 ± 0.015; 0.025	1.740	171.07
2.0	1.34 ± 0.012; 0.021	1.550	173.13
3.0	1.23 ± 0.012; 0.020	1.626	175.40
4.0	1.23 ± 0.015; 0.025	2.052	175.47

Table 4 The effect of gram MIP on the binding capacity

MIP (g)	C_e(μg mL^{-1}) ± SE; SD (n = 3)	RSD	Q(μg g^{-1})
0.1	9.225 ± 0.009; 0.015	0.165	75.33
0.3	5.71 ± 0.018; 0.031	0.535	143.11
0.5	1.23 ± 0.015; 0.025	2.052	175.47
0.7	1.23 ± 0.020; 0.035	2.863	175.47

Table 5 The maximum binding capacity (Q_{max}) and imprinting factor (IF) obtained from the Scatchard plot for TNX

Polymers	K_d	Q_{max}(μg.g^{-1})	IF
MIP-high	0.049	230.93	1.89
MIP-low	1.28	479.83	3.92
NIP	0.088	122.48	–

in MIPs then steadily diffused outward until the release rate reached its maximum. The synthetic MIP is a good drug vehicle as it does not have a burst release effect.

In general, drug release at pH 1 was faster than at pH 6.8 and 7.4. Diffusion through matrix swelling and dissolution/erosion at the matrix periphery controls drug release. The "swelling–dissolution–erosion" cycle is a complicated one. The osmotic pressure differential that exists between the alginate gel and the environment is a key element in the swelling process in systems based on sodium alginate crosslinked with calcium chloride. Swelling of the calcium alginate beads is rare under acidic circumstances (e.g., in the stomach) (Tønnesen and Karlsen 2002). The physicochemical properties of TNX helped to explain this phenomenon. In a pH 1 setting, alginate could form particulate and absorbent structures on the surface media. Swelling of TNX at pH 1 may compensate for this structural defect, enhancing the ability to control release.

However, TNX is gradually released over time due to alginate corrosion and minor breakdown at pH 6.8. The rate of drug release at pH 7.4 is supposed to be higher than at pH 1 and lower than at pH 6.8. However, aberrant results were detected in the release summaries, which could be linked to the new mechanism of the TNX-alginate-based environment. At pH 1, TNX was released from the TNX/MIP medium, followed by pH 6.8, and finally pH 7.4.

Table 7 In vitro TNX-release kinetics at various pHs using the *Higuchi* model

pH	Regression equation	R^2
1.0	M_t/M_∞	0.8355
6.8	$M_t/M_\infty = 6.2781\sqrt{t} + 47.685$	0.9009
7.4	$M_t/M_\infty = 6.0120\sqrt{t} + 27.649$	0.9161

Analytical application

Pharmaceuticals in the form of tenoxicam capsules were used to test the proposed approach. Different volumes of pharmaceutical solutions were taken to make a final volume of 10 mL. The separation process was done using MIP and NIP under ideal conditions, and the results are shown in Table 8.

Conclusion

In conclusion, a new method to synthesize molecular imprinted polymer (MIP) in nanoscale size from alginate was established, and it was applied to the extraction and estimation of tenoxicam (TNX) in pharmaceutical formulations. Although alginates have been used as tools in

Table 6 Selectivity adsorption of the MIP to TNX

Matrix (10 μg mL^{-1})	**TNX** (C_o = 10 μg mL^{-1})				
PRO	MIP	C_e(μg.mL^{-1}) ± SE; SD (n = 3)	Q(μg.g^{-1})	Recovery*	RSD
		0.4 ± 0.006; 0.010	192.00	96.00	2.500
	NIP	6.38 ± 0.046; 0.080	72.40	36.20	1.254
NIC	MIP	0.25 ± 0.003; 0.006	195.07	97.53	2.341
	NIP	6.45 ± 0.081; 0.140	70.93	35.47	2.177

*The recovery was calculated for the TNX that was retained in the MIP and NIP

Table 8 Application of the proposed method to the separation and determination of TNX in pharmaceutical sample, recovery values are equal to the extraction efficiency

Sample	Taken TNX ($\mu g\ mL^{-1}$)		C_e($\mu g\ mL^{-1}$) ± SE; SD ($n=3$)	Q	Recovery	RSD
Tenoksan Capsule (20 mg/Capsule)	7	MIP	0.80 ± 0.012; 0.20	124.0	88.57	2.500
		NIP	4.31 ± 0.047; 0.082	53.8	38.43	1.903
	10	MIP	1.17 ± 0.012; 0.012	176.6	88.30	1.795
		NIP	5.95 ± 0.019; 0.033	81.0	40.50	0.555
	13	MIP	2.01 ± 0.012; 0.007	219.8	84.54	0.597
		NIP	7.64 ± 0.021; 0.036	107.2	41.23	0.471

a variety of pharmaceutical and biomedical applications, no pharmaceutical claims have been made on the alginate molecule itself. The approach proved easy to use, effective, and drug-responsive. This particular polymer can be made in either a neutral or a charged state, and with or without metal crosslinkers, making it suitable for a wide range of applications. Alginate is generally thermally stable in neutral conditions. The design of the molecule in drug delivery has enabled the development of systems capable of regulating drug release according to physiological needs due to its varied reactivity to different pHs. Alginates possess adequate physical and chemical characteristics to contribute significantly to this sector.

Declarations

Conflicts of interest There are no conflicts to declare.

References

Abdeen R, Salahuddin N (2013) Modified chitosan-clay nanocomposite as a drug delivery system intercalation and in vitro release of ibuprofen. J Chem. https://doi.org/10.1155/2013/576370

Abood ME, Abbas SM (2021) Molecular imprinted of nylon 6 for selective separation of procaine by solid-phase extraction. Indones J Chem 21. https://doi.org/10.22146/ijc.66997

Ahmad Z, Pandey R, Sharma S, Khuller G (2006) Alginate nanoparticles as antituberculosis drug carriers: formulation development, pharmacokinetics and therapeutic potential. Indian J Chest Dis Allied Sci 48:171

Al-Abbasi M, Al-Bayati Y, Al-Samarrai K (2020) Synthesis Of molecularly imprinted polymers (Mips) Used For estimation of betamethasone disodium phosphate (Bmsp) Using different functional monomers. Iraqi J Agri Sci 51:483–492

Al-Bayati YK, Al-Safi AJ (2018) Synthesis and characterization of a molecularly imprinted polymer for diclofenac sodium using (2-vinylpyridine and 2-hydroxyethyl metha acrylate) as the complexing monomer. Baghdad Sci J 15:63–72https://doi.org/10.21123/bsj.2018.15.1.0063

Alkhatib H, Mohamed F, Akkawi ME, Alfatama M, Chatterjee B, Doolaanea AA (2020) Microencapsulation of black seed oil in alginate beads for stability and taste masking. J Drug Delivery Sci Technol 60:102030

Amin AS (2002) Spectrophotometric determination of piroxicam and tenoxicam in pharmaceutical formulations using alizarin. J Pharm Biomed Anal 29:729–736

Arslan H, Topcuoglu HS, Aladag H (2011) Effectiveness of tenoxicam and ibuprofen for pain prevention following endodontic therapy in comparison to placebo: a randomized double-blind clinical trial. J Oral Sci 53:157–161

Bereli N, Akgönüllü S, Asliyüce S, Çimen D, Göktürk İL, Türkmen D, Yavuz H, Denizli A (2020) Molecular imprinting technology for biomimetic assemblies. Hacettepe J Biol Chem 48:575–601

Chandra Mohan PD (2003) Buffers. A guide for the preparation and use of buffers in biological systems. CALBIOCHEMfi EMD Biosciences, Inc., An Affiliate of Merck KGaA, Darmstadt, Germany

Cetinkaya A, Yildiz E, Kaya SI, Çorman ME, Uzun L, Ozkan SA (2022) A green synthesis route to develop molecularly imprinted electrochemical sensor for selective detection of vancomycin from aqueous and serum samples. Green Anal Chem 2:100017

Chan L, Jin Y, Heng P (2002) Cross-linking mechanisms of calcium and zinc in production of alginate microspheres. Inter J Pharm 242:255–258

Chen S, Zhao F (2012) Highly sensitive chemiluminescence determination of tenoxicam using a cerium (IV)–sodium hyposulphite system in micellar medium. Luminescence 27:279–284

Chen JH, Li GP, Liu QL, Ni JC, Wu WB, Lin JM (2010) Cr (III) ionic imprinted polyvinyl alcohol/sodium alginate (PVA/SA) porous composite membranes for selective adsorption of Cr (III) ions. Chem Eng J 165:465–473

Ciurba A, Antonoaea P, Todoran N, Rédai E, Vlad R, Tataru A, Muntean D, Bîrsan M (2021a) Polymeric films containing tenoxicam as prospective transdermal drug delivery systems: design and characterization. Processes 9:136

Ciurba A, Antonoaea P, Todoran N, Rédai E, Vlad RA, Tătaru A, Muntean D-L, Bîrsan M (2021b) Polymeric films containing tenoxicam as prospective transdermal drug delivery systems: design and characterization. Processes 9:136

Daemi H, Barikani M (2012) Synthesis and characterization of calcium alginate nanoparticles, sodium homopolymannuronate salt and its calcium nanoparticles. Scientia Iranica 19:2023–2028

Decompte E, Lobaz V, Monperrus M, Deniau E, Save M (2020) Molecularly imprinted polymer colloids synthesized by miniemulsion polymerization for recognition and separation of nonylphenol. ACS Appl Polymer Mater 2:3543–3556

Demiralay EÇ, Yilmaz H (2012) Potentiometric pKa determination of piroxicam and tenoxicam in acetonitrile-water binary mixtures. Süleyman Demirel Üniversitesi Fen Edebiyat Fakültesi Fen Dergisi 7:34–44

El-Gazayerly ON (2000) Characterization and evaluation of tenoxicam coprecipitates. Drug Dev Ind Pharm 26:925–930

Gao Z, Zeng Q, Wang M, Wang L (2022) Sensitive Detection of 8-Hydroxyquinoline in Cosmetics by Using a Poly (tannic acid)-Modified Glassy Carbon Electrode. Chem Select 7:e202200257

Geetha P, Latha M, Pillai SS, Deepa B, Kumar KS, Koshy M (2016) Green synthesis and characterization of alginate nanoparticles and its role as a biosorbent for Cr (VI) ions. J Mol Struct 1105:54–60

Haldar K, Chakraborty S (2019) Investigation of chemical reaction during sodium alginate drop impact on calcium chloride film. Phys Fluids 31:072102

Hamed S, Ayob F, Alfatama M, Doolaanea AA (2017) Enhancement of the immediate release of paracetamol from alginate beads. Inter J Appl Pharm 9:47–51

Hasseb AA, Shehab OR, El Nashar RM (2022) Application of molecularly imprinted polymers for electrochemical detection of some important biomedical markers and pathogens. Curr Opin Electrochem 31:100848

Herrero EP, Martín Del Valle EM, Peppas NA (2010) Protein imprinting by means of alginate-based polymer microcapsules. Ind Eng Chem Res 49:9811–9814

Hou S, Wang Y, Liu N, Liu J (2014) Preparation and recognition characteristics of thymopentin molecularly imprinted polymers on SiO2. Adsorpt Sci Technol 32:833–843

Huang Y-J, Chang R, Zhu Q-J (2018) Synthesis and characterization of a molecularly imprinted polymer of spermidine and the exploration of its molecular recognition properties. Polymers 10:1389

Hussein HJ, Al-Bayati YK (2021) Determination Of Cefalaxin In Pharmaceutical Preparation Bymoleculary Imprented Polymer In Pvc Matrix Membrane. Iraqi J Market Res Consumer Protect 13:159–172

Jaoued-Grayaa N, Nasraoui C, Chevalier Y, Hbaieb S (2022) Design of molecularly imprinted polymer materials relying on hydrophobic interactions. Colloids Surf, A 647:129008

Kurczewska J (2022) Recent Reports on Polysaccharide-Based Materials for Drug Delivery. Polymers 14:4189

Liu D, Zhao K, Qi M, Li S, Xu G, Wei J, He X (2018) Preparation of protein molecular-imprinted polysiloxane membrane using calcium alginate film as matrix and its application for cell culture. Polymers 10:170

Madni MA, Raza A, Abbas S, Tahir N, Rehman M, Kashif PM, Khan MI (2016) Determination of tenoxicam in the plasma by reverse phase HPLC method using single step extraction technique: a reliable and cost effective approach. Acta Pol Pharm 73:1129–1134

Mokhtari P, Ghaedi M (2019) Water compatible molecularly imprinted polymer for controlled release of riboflavin as drug delivery system. Eur Polymer J 118:614–618

Nantasenamat C, Isarankura-Na-Ayudhya C, Naenna T, Prachayasittikul V (2007) Quantitative structure-imprinting factor relationship of molecularly imprinted polymers. Biosens Bioelectron 22:3309–3317

Prabaharan M (2015) Chitosan-based nanoparticles for tumor-targeted drug delivery. Int J Biol Macromol 72:1313–1322

Puoci F, Iemma F, Picci N (2008) Stimuli-responsive molecularly imprinted polymers for drug delivery: a review. Curr Drug Deliv 5:85–96

Qi M, Zhao K, Bao Q, Pan P, Zhao Y, Yang Z, Wang H, Wei J (2019) Adsorption and electrochemical detection of bovine serum albumin imprinted calcium alginate hydrogel membrane. Polymers 11:622

Rastogi R, Sultana Y, Aqil M, Ali A, Kumar S, Chuttani K, Mishra A (2007) Alginate microspheres of isoniazid for oral sustained drug delivery. Int J Pharm 334:71–77

Sarpong KA, Xu W, Huang W, Yang W (2019) The development of molecularly imprinted polymers in the clean-up of water pollutants: a review. Am J Anal Chem 10:202–226

Scatchard G (1949) The attractions of proteins for small molecules and ions. Ann NY Acad Sci 51:660–672

Shalapy A, Zhao S, Zhang C, Li Y, Geng H, Ullah S, Wang G, Huang S, Liu Y (2020) Adsorption of deoxynivalenol (DON) from corn steep liquor (CSL) by the microsphere adsorbent SA/CMC loaded with calcium. Toxins 12:208

Smrdel P, Bogataj M, Podlogar F, Planinšek O, Zajc N, Mazaj M, Kaučič V (2006) Characterization of calcium alginate beads containing structurally similar drugs. Drug Dev Ind Pharm 32:623–633

Szatkowska P, Koba M, Koslinski P, Szablewski M (2013) Molecularly imprinted polymers' applications: A short review. Mini-Rev Org Chem 10:400–408

Tamayo F, Turiel E, Martín-Esteban A (2007) Molecularly imprinted polymers for solid-phase extraction and solid-phase microextraction: Recent developments and future trends. J Chromatogr A 1152:32–40

Tønnesen HH, Karlsen J (2002) Alginate in drug delivery systems. Drug Dev Ind Pharm 28:621–630

Wu J, Zeng RJ, Zhang F, Yuan Z (2019) Application of iron-crosslinked sodium alginate for efficient sulfide control and reduction of oilfield produced water. Water Res 154:12–20

You J-Z, Wu C-J, Wang X-J (2018) The thermal decomposition mechanism and kinetics of tenoxicam. J Anal Appl Pyrol 134:573–579

Zhang W, She X, Wang L, Fan H, Zhou Q, Huang X, Tang JZ (2017a) Preparation, characterization and application of a molecularly imprinted polymer for selective recognition of sulpiride. Materials 10:475

Zhang W, Wei B, Li S, Wang Y, Wang S (2017b) Preparation and Chromatographic Application of β-cyclodextrin molecularly imprinted microspheres for paeoniflorin. Polymers 9:214

Zhang W, Li Q, Cong J, Wei B, Wang S (2018) Mechanism analysis of selective adsorption and specific recognition by molecularly imprinted polymers of Ginsenoside Re. Polymers 10:216

Zhao K, Feng L, Lin H, Fu Y, Lin B, Cui W, Li S, Wei J (2014) Adsorption and photocatalytic degradation of methyl orange imprinted composite membranes using TiO2/calcium alginate hydrogel as matrix. Catal Today 236:127–134

Zhu Y, Yang L, Huang D, Zhu Q (2017) Molecularly imprinted nanoparticles and their releasing properties bio-distribution as drug carriers. Asia J Pharm Sci 12:172–178